PCCP

Accepted Manuscript

This is an *Accepted Manuscript*, which has been through the Royal Society of Chemistry peer review process and has been accepted for publication.

Accepted Manuscripts are published online shortly after acceptance, before technical editing, formatting and proof reading. Using this free service, authors can make their results available to the community, in citable form, before we publish the edited article. We will replace this *Accepted Manuscript* with the edited and formatted *Advance Article* as soon as it is available.

You can find more information about *Accepted Manuscripts* in the **Information for Authors**.

Please note that technical editing may introduce minor changes to the text and/or graphics, which may alter content. The journal's standard **Terms & Conditions** and the **Ethical guidelines** still apply. In no event shall the Royal Society of Chemistry be held responsible for any errors or omissions in this *Accepted Manuscript* or any consequences arising from the use of any information it contains.

ARTICLE

A Novel Apatite, Lu$_5$(SiO$_4$)$_3$N:(Ce, Tb) Phosphor Materials: Synthesis, Structure and Applications for NUV-LEDS

Qingfeng Guo,[a] Qidi Wang,[b] Liwei Jiang,[c] Libing Liao[*,a] Haikun Liu[a], Lefu Mei[a]

Abstract: The lutetium containing nitride apatite, Lu$_5$(SiO$_4$)$_3$N was prepared by a solid state reaction at high temperature for the first time. Rietveld refinement indicated that Lu$_5$(SiO$_4$)$_3$N compound has a hexagonal space group $P6_3/m$ with cell parameters $a = b$ = 9.700 Å and c = 7.238 Å. Additionally, the results revealed that there are two distinct lutetium sites in the Lu$_5$(SiO$_4$)$_3$N host lattice, i.e., Lu(1) site with nine coordination (Wyckoff site 4f) and Lu(2) site with seven coordination (Wyckoff site 6h). Furthermore, the ratio of the number of Lu atoms in Lu(1) and Lu(2) sites is 3:2. The band gap for Lu$_5$(SiO$_4$)$_3$N was determined to be 4.12 eV based on the density functional theory (DFT). In the Ce^{3+} doped Lu$_5$(SiO$_4$)$_3$N: 0.03Ce^{3+} compound, the emission peak centered at 462 nm was observed with the Commission International de I'Eclairage (CIE) coordinates of (0.148, 0.184), indicating blue-emission. Remarkably, in Ce^{3+} and Tb^{3+} co-doped Lu$_{4.97-y}$(SiO$_4$)$_3$N: 0.03Ce^{3+}, yTb^{3+} compounds, the color-tunability was observed with increasing Tb^{3+} co-doping rate on moving from blue at Tb^{3+} = 0.00 to green at Tb = 0.09, due to the energy transfer from Ce^{3+} to Tb^{3+} ions being matched well with the decay curve results. Under the excitation of 359 nm, the absolute quantum efficiency (QE) for Lu$_5$(SiO$_4$)$_3$N: 0.03Ce^{3+} was determined to be 42.13%. This phosphor material could be a platform for modeling a new phosphor and application in the solid-state lighting field.

1. Introduction

Apatite compounds have been investigated as effective luminescent host materials in recent years because of their physical and chemical stability. Therefore, they have been widely used in lighting and display areas.[1-4] Apatite belongs to hexagonal crystal system represented generally as M$_{10}$(XO$_4$)$_6$Z$_2$ (M = Ca^{2+}, Sr^{2+}, Ba^{2+}, K+, Na+, Ce^{3+}, La^{3+}, Y^{3+}, etc., X = P^{5+}, Si^{4+}, S^{6+}, V^{5+}, etc., and Z = O^{2-}, F$^-$, Cl$^-$, Br$^-$, OH$^-$, S^{2-}, etc.).[5,6] In general, there are two kinds of non-equivalent crystallographic sites in apatite compounds, that is, the nine-coordinated 4f site M(I) with C_3 point symmetry and the seven-coordinated 6h site M(II) with C_s point symmetry, respectively.[7,8] Thus, it is interesting and significant to do research on the relationship between structure (substitution) and luminescence properties in apatite structure. Accordingly, many efforts have been made to obtain novel phosphors on the basis of different chemical compositions, such as Sr$_{10}$(PO$_4$)$_6$O: Eu^{2+},[9] Sr$_3$GdNa(PO$_4$)$_3$F: Eu^{2+}, Mn^{2+},[10] Ca$_9$Mg(PO$_4$)$_6$F$_2$: Eu^{2+}, Mn^{2+}.[11]
Meanwhile, the wavelength of excitation and emission bands for phosphors with oxonitridosilicate structure are even longer than that of other phosphors because of their high covalency and strong crystal fields. (Si[O/N]$_4$) units are stacked together by sharing their corners and edges forming a condensed (Si[O/N]$_4$) frameworks, making oxonitridosilicates excellent hosts for rare earth ions. Therefore, oxonitridosilicates have been used as hosts to obtain phosphors, such as: Y$_{10}$(Si$_6$O$_{22}$N$_2$)O$_2$: Ce^{3+}, Mn^{2+},[12] Ca$_3$Si$_2$O$_4$N$_2$: Eu^{2+},[13] Y$_4$Si$_2$O$_7$N$_2$: Eu^{2+}.[14] Besides, the luminescence properties of Ce^{3+} ions can be strongly affected by their surrounding crystal field environment, due to their 5d electrons unshielded from the crystal field by the 5s and 5p electrons in the excited state. Thus, Ce^{3+} doped oxonitridosilicates have been widely investigated, such as Ca$_3$Si$_2$O$_4$N$_2$: Ce^{3+},[15] Y$_5$(SiO$_4$)$_3$N: Ce^{3+},[16] Sr$_3$Si$_2$O$_4$N$_2$: Ce^{3+},[17] Gd$_5$Si$_3$O$_{12}$N: Ce^{3+}.[18] Among oxonitridosilicates, Lu-Si-O-N quaternary system compounds have been investigated in the previous literatures, such as Lu$_4$Si$_2$O$_7$N$_2$.[19,20] However, to the best of our knowledge, Lu$_5$(SiO$_4$)$_3$N compound (oxonitridosilicate) has not been identified and reported before.
In the light of the above, a novel oxonitridosilicate Lu$_5$(SiO$_4$)$_3$N with apatite structure was obtained for the first time under 0.5 MPa atmosphere pressure. The crystal structure properties of Lu$_5$(SiO$_4$)$_3$N were studied in detail. Rietveld refinement indicated that Lu$_5$(SiO$_4$)$_3$N compound has a hexagonal space

a. Beijing Key Laboratory of Materials Utilization of Nonmetallic Minerals and Solid Wastes, National Laboratory of Mineral Materials. School of Materials Sciences and Technology, China University of Geosciences, Beijing 100083, China
b. School of Earth Sciences and Resources, China University of Geosciences, Beijing 100083, China
c. Key Laboratory for Renewable Energy, Beijing Key Laboratory for New Energy Materials and Devices, Beijing National Laboratory for Condensed Matter Physics, Institute of Physics, Chinese Academy of Sciences, Beijing 100190, China
Corresponding author: Libing Liao E-mail: clayl@cugb.edu.cn
Phone: +86-10-8233-1701 Fax:+86-10-8233-1701
Electronic Supplementary Information (ESI) available: Crystallographic information files (CIF) of the Lu$_5$(SiO$_4$)$_3$N compound.
See DOI: 10.1039/x0xx00000x

ARTICLE

group $P6_3/m$ with cell parameters $a = b = 9.700$ Å and $c = 7.238$ Å. Two distinct lutetium sites in the $Lu_5(SiO_4)_3N$ host lattice, i.e., Lu(1) site with nine coordination (Wyckoff site $4f$) and Lu(2) site with seven coordination (Wyckoff site $6h$) were revealed, and the ratio of the number of Lu atoms in Lu(1) and Lu(2) sites is 3:2. The band gap for $Lu_5(SiO_4)_3N$ was determined to be 4.12 eV based on the density functional theory (DFT). In addition, the luminescence properties and energy transfer behaviors between Ce^{3+} and Tb^{3+} were investigated systematically. The results indicated that $Lu_5(SiO_4)_3N$ phosphor material could be a platform for modeling a new phosphor and application in the solid-state lighting field.

2. Experimental Procedure

2.1 Materials and Synthesis

$Lu_5(SiO_4)_3N$ host and $Lu_5(SiO_4)_3N:Ce^{3+},Tb^{3+}$ phosphors were prepared by a high temperature solid-state reaction. SiO_2 (Aldrich, 99.9%), α-Si_3N_4 (Aldrich, 99.9%), Lu_2O_3 (Aldrich, 99.995%), CeO_2 (Aldrich, 99.995%), and Tb_4O_7 (Aldrich, 99.995%) were weighted and used as starting materials according to the given composition of $Lu_5(SiO_4)_3N:Ce^{3+},Tb^{3+}$. The raw materials were fully mixed and ground in an agate mortar, and the mixture was placed into an alumina crucible and was heated at 1500 °C for 5 h in a reducing atmosphere with flowing gas (10% H_2 + 90% N_2) and 0.5 MPa atmosphere pressure. Eventually, the obtained samples were cooled to room temperature and ground again into powder for subsequent measurements.

2.2 Characterization

Phase structures of the as-prepared samples were checked by X-ray powder diffractometer (D/max-rA 12kw, Japan) with Cu Kα radiation (λ = 1.5418 Å) from 10° to 70° (2θ). The XRD data for the Rietveld analysis were collected in a step scanning mode with a step size of 0.02 ° and 3 s counting time per step from 10° to 75° (2θ). Rietveld refinement was performed using the computer software: General Structure Analysis System (GSAS).[21] Computations were performed within the density functional theory (DFT) framework, with the Vienna *ab* initio software package (VASP), within the generalized gradient approximation by Perdew-Burke-Ernzher of (GGA-PBE) and projector augmented wave pseudopotentials (PAW). A cutoff energy of 520 eV and appropriate k-point grid was chosen to ensure that total energies converged within 10^{-4} eV per formula unit. The supercell of $Lu_5(SiO_4)_3N$ used in this study includes 42 atoms. When the structures were optimized, all atoms were allowed to relax. Since the optimized lattices of the systems were determined by several structure parameters,

it is time consuming to get the theoretical value of these parameters through the traditional DFT calculation. In this work, the structures were optimized until all residual forces were below 0.001 eV/Å. Brillouin-zone integrations were performed using Monkhorst-Pack grids of special points with a mesh (2× 2 × 3).[22] The room-temperature excitation and emission spectra were measured on a Hitachi F-4500 spectrophotometer with a 150 W Xe lamp as the excitation lamp. The luminescence decay curves were obtained on a spectro-fluorometer (HORIBA JOBIN YVON FL3-21), and the 370 nm pulse laser radiation (370-nm Nano LED, model number 08254) was used as the excitation source. The particle morphology and microstructure of the $Lu_5(SiO_4)_3N$ and $Lu_{4.97}(SiO_4)_3N$: 0.03Ce^{3+} samples were examined by scanning electron microscopy (SEM) using a HitachiS-520, instrument with an accelerating voltage of 25 kV. The results of element analysis were gotten from an energy dispersive X-ray spectrometer (EDS) attached to the scanning electron microscope. The quantum efficiency (QE) was obtained by the absolute photoluminescence quantum yield measurement system (FluoroLog-3-2-iHR320, Horiba Jobin Yvon) with F-3018 integral sphere at room temperature.

3. Results and Discussion

3.1 Insight into $Lu_5(SiO_4)_3N$

Table 1. Refinement parameters for $Lu_5(SiO_4)_3N$ obtained from the Rietveld refinement using X-ray powder diffraction data at room temperature.

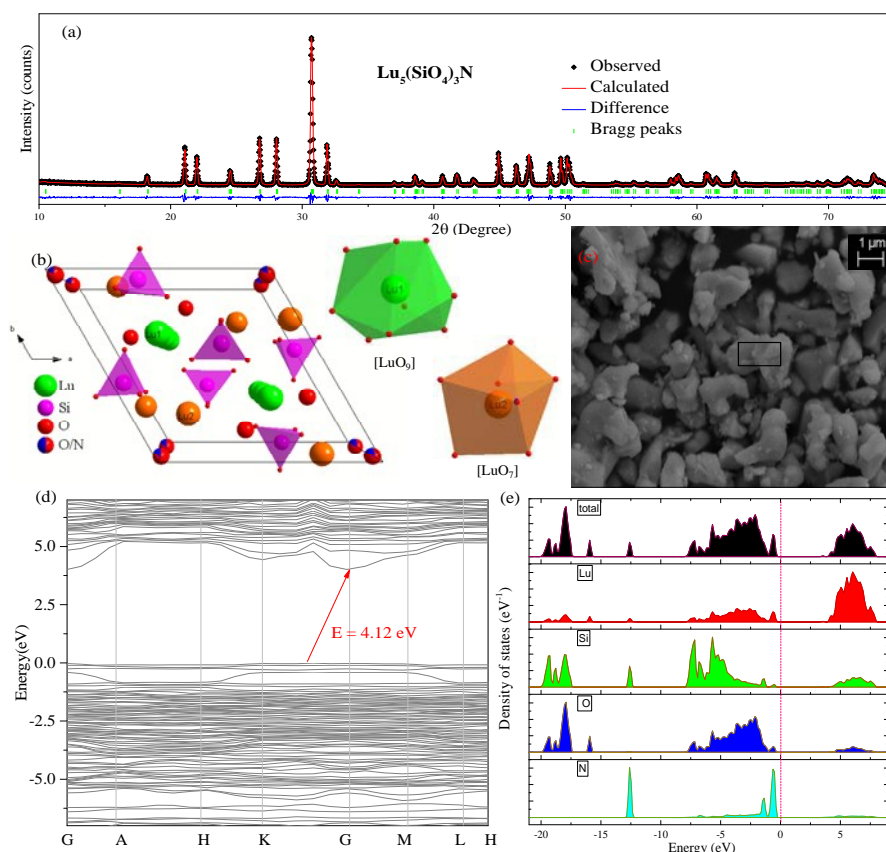| Sample	$Lu_5(SiO_4)_3N$
Space group	$P6_3/m$(176)
a, Å	9.7005(17)
c, Å	7.2383(3)
V, Å^3	589.87(4)
2θ-interval, °	10-75
R_{wp}, %	8.88
R_p, %	5.99
χ^2	1.63

Figure 1. Powder XRD patterns for the Rietveld refinement analysis of $Lu_5(SiO_4)_3N$. Solid red lines are calculated intensities, and the black square points are the observed intensities, and blue solid lines stand for the difference between the observed and the calculated intensities, and short green vertical lines below the profiles stand show the position of Bragg reflections of the calculated pattern **(a)**; Crystal structure diagrams of $Lu_5(SiO_4)_3N$ viewed in the *c*-direction and the coordination environment of cation sites for activators **(b)**; SEM image of $Lu_5(SiO_4)_3N$ **(c)**; Calculated band structure of $Lu_5(SiO_4)_3N$ **(d)**; Electronic densities of states for $Lu_5(SiO_4)_3N$, both total (TDOS) and partial (PDOS) onto atomic orbital **(e)**.

Figure 1 (a) shows the Rietveld structural refinement of the XRD pattern of the $Lu_5(SiO_4)_3N$ host using the GSAS program. As depicted in Figure 1(a), the red solid line, black square points, green short vertical and blue lines represent the calculated pattern, observed pattern from experiment, the Bragg positions of the calculated pattern, and the difference between the observed and calculated patterns, respectively. It is obvious that almost all the peaks of $Lu_5(SiO_4)_3N$ can be indexed by hexagonal cell ($P6_3/m$). In addition, $Lu_5(SiO_4)_3N$ has similar XRD patterns with $La_5(SiO_4)_3N$ (apatite structure, ICSD no. 91850), which have been widely investigated.[23-25] Therefore, $La_5(SiO_4)_3N$ was taken as starting model structure for Rietveld refinement. The refinement was stable and gives low *R*-factors (Figure 1 (a), Table 1), and the final refinement residual factors are R_{wp} = 8.88%, R_p = 5.99%, and χ^2 = 1.63. Besides, the refinement results further confirm that the single-phase compound $Lu_5(SiO_4)_3N$ can be indexed in the hexagonal space group $P6_3/m$ with cell parameters $a = b$ = 9.7005 Å, c = 7.2383 Å and V = 589.87 Å^3. Furthermore, the fractional atomic coordinates, isotropic displacement parameters (Å^2), as well as the main bond lengths (Å) for $Lu_5(SiO_4)_3N$ are illustrated in Table 2 and Table 3. According to Table 2, O1 is located on site 2a with -6 site symmetry, while Si1, O2, and O3 are located

on the mirror planes with site symmetry m (site 6*h*). O4 and N4 are on a general positon (site 12*i*). Based on the results from Table 3, the average bond length of Lu(1)-O/N can be calculated to be 2.706 Å, and 2.543 Å for Lu(2) sites. Besides, the crystallographic information files (CIF) of $Lu_5(SiO_4)_3N$ was also illustrated in the Electronic Supplementary Information (ESI). Figure 1 (b) illustrates the crystal structure of $Lu_5(SiO_4)_3N$ view along the *c*-axis, and the coordination environment of cation sites for activators were also given. In the crystal lattice of this compound, Si atoms are tetrahedral coordinated to form [SiO$_4$] groups, which are isolated from each other. $Lu_5(SiO_4)_3N$ contains two non-equivalent lutetium sites, where Lu(1) is located on a 3-fold axis (Wyckoff symbol 4*f*), while Lu(2) is located on a mirror plane (site 6h). Lu(1) are nine coordinated by O/N atoms forming a tricapped trigonal-prismatic geometry, but Lu(2) are seven coordinated by O/N atoms forming an irregular polyhedron, respectively. Furthermore, the ratio of the number of Lu atoms in the two sites is 3:2.

The morphology of $Lu_5(SiO_4)_3N$ host prepared via solid state reaction is shown in in Figure 1 (c). SEM result shows that particles of the as-prepared sample are not uniform, which was caused by the agglomeration during the sample sintering.

Table 2. Structural parameters for $Lu_5(SiO_4)_3N$ obtained from the Rietveld refinement using X-ray powder diffraction data at room temperature.

	Wyck	x	y	z	U (Å^2)	Occupation
Lu1	*4f*	0.2310(8)	-0.0153(9)	1/4	0.0158	1
Lu2	*6h*	1/3	2/3	0.0007(4)	0.0249	1
Si1	*6h*	0.3932(5)	0.3788(1)	1/4	0.0017	1
O1	*2a*	0	0	1/4	0.0568	1
O2	*6h*	0.3308(8)	0.4682(7)	1/4	0.0143	1
O3	*6h*	0.5871(9)	0.4731(6)	1/4	0.0014	1
O4	*12i*	0.3443(2)	0.2570(5)	0.0769(2)	0.0027	5/6
N4	*12i*	0.3443(2)	0.2570(5)	0.0769(2)	0.0027	1/6

Additionally, the SEM image indicated that the sample has a well-crystallized microporous with the diameter of about 3-6 μm. In order to confirm the chemical composition of the $Lu_5(SiO_4)_3N$, the as-prepared sample was analysed by energy dispersive spectroscopy (EDS) analysis. Table 4 shows the results of EDS element analysis (wt%) within the rectangle area in Figure 1 (c). As illustrated in Table 4, La, Si, O, and N exist in the host $Lu_5(SiO_4)_3N$. Besides, the weight ratio of each element in $Lu_5(SiO_4)_3N$ is Lu 70.80%, Si 7.06%, O 19.21% and N 2.93% according to the EDS results in Table 4.

The band structure of pure $Lu_5(SiO_4)_3N$ calculated by using VASP is presented in Figure 1 (d). The results reveal that the valence band maximum (VBM) and the conduction band minimum (CBM) are at different points, indicating that $Lu_5(SiO_4)_3N$ has an indirect broad band gap. In addition, the band gap was determined to be approximately 4.12 eV. As we

Table 3. Main bond lengths (Å) of $Lu_5(SiO_4)_3N$ from Rietveld structure analysis, and the symmetry codes of the matching O/N element.

Bond	Lengths (Å)	Symmetry codes	Bond	Lengths (Å)	Symmetry codes
Lu2-O1	2.3198(1)	*x, y, z*	Lu1-O3	2.6027(1)	*x-y, x, -0.5+z*
Lu2-O2	2.7223(1)	*-x+y, -x, z*	Lu1-O3	2.6027(1)	*1-x, 1-y, -0.5+z*
Lu2-O3	2.4911(1)	*1-y, x-y, z*	Lu1-O3	2.6027(1)	*y, 1-x+y, -0.5+z*
Lu2-O4/N4	2.6187(1)	*x, y, z*	Lu1-O4/N4	2.8857(1)	*1-x, 1-y, -z*
Lu2-O4/N4	2.5149(1)	*y, -x+y, 0.5+z*	Lu1-O4/N4	2.8857(1)	*y, 1-x+y, -z*
Lu2-O4/N4	2.5149(1)	*y, -x+y, -z*	Lu1-O4/N4	2.8857(1)	*x-y, x, -z*
Lu2-O4/N4	2.6187(1)	*x, y, 0.5-z*	Si1-O2	1.2823(1)	*x, y, z*
Lu1-O2	2.6294(1)	*x, y, z*	Si1-O3	1.6295(1)	*x, y, z*
Lu1-O2	2.6295(1)	*1-y, 1+x-y, z*	Si1- O4/N4	1.6215(0)	*x, y, z*
Lu1-O2	2.6294(1)	*-x+y, 1-x, z*	Si1- O4/N4	1.6215(0)	*x, y, 0.5-z*

Table 4. The results of Energy dispersive spectroscopy (EDS) element analysis (*wt*%) of $Lu_5(SiO_4)_3N$ sample within the rectangle area in Figure 1(c) and $Lu_5(SiO_4)_3N$: $0.03Ce^{3+}$ within the rectangle area in Figure 3(d).

$Lu_5(SiO_4)_3N$			$Lu_{4.97}(SiO_4)_3N$: $0.03Ce^{3+}$		
Element	Weight (%)	Atomic (%)	Element	Weight (%)	Atomic (%)
Lu	70.80	23.13	Lu	70.63	23.07
Si	7.06	12.20	Ce	0.15	0.22
O	19.21	56.32	Si	7.24	12.51
N	2.93	8.35	O	18.96	55.59
			N	3.02	8.61
Total	100.00	100.00	Total	100.00	100.00

know, electronic densities of states analysis were considered an effective way to assign the band structure and analyze the bonding interactions in the crystal. Therefore, the electronic densities of states of $Lu_5(SiO_4)_3N$, both total (TDOS) and partial (PDOS) onto atomic orbital were performed as illustrated in Figure 1 (e). It can be seen that the valence bands in the range of -19.89 to -17.35 eV originate from O, Si, and Lu. The peaks at about -15.93 eV correspond to Lu and O states bands. Furthermore, the valence bands close to Fermi level (-0.61 to 0 eV) are dominated by the states of O and N. Finally, the conduction band (below 6.5 eV) is dominated by states of Lu. Therefore, the band gap of $Lu_5(SiO_4)_3N$ is determined by O/N and Lu atoms.

3.2 Luminescence properties of $Lu_5(SiO_4)_3N$: Ce^{3+} phosphor

Figure 2 depicts the photoluminescence excitation (PLE) and emission (PL) spectra of $Lu_{5-x}(SiO_4)_3N$: xCe^{3+} (a), and the relative emission intensity and emission peak maximum (nm) as a function of Ce^{3+} concentration (b). Under the excitation at 359 nm, $Lu_{5-x}(SiO_4)_3N$: xCe^{3+} exhibit a broad blue emission band peaking at about 460 nm. The PLE spectrum monitored at 462 nm shows a broad absorption from 245 to 400 nm, including two obvious broad bands centered at 314 and 359 nm attributed to $4f{\rightarrow}5d$ transition of Ce^{3+}.[26, 27] As depicted in Figure 2 (a) and (b), the emission intensity of Ce^{3+} increased firstly with the Ce^{3+} concentration x, and achieved the maximum value at $x = 0.03$ (mol), and then it decreased dramatically with further increase of concentration, which may be attributed to the concentration quenching effect. Therefore, the optimum doping concentration x of Ce^{3+} is 0.03. Moreover, the emission peak shows slight red shift from 454 to 464 nm with increasing of Ce^{3+} concentration, which may be due to the variation of crystal field strength. In addition, the correlation between the crystal field splitting (D_q) and the shape and size of the polyhedron is given by the following equation:[28]

$$D_q = \frac{Ze^2r^4}{6R^5} \qquad (1)$$

where D_q refers to the energy level separation, z is the charge or valence of the anion ligand, e stands for the charge of an electron, r represents the radius of the d wave function, and R represents the bond length. Assuming that z, e and r are the same for d(Ce-O)-orbital and d(Ce-N)-orbital, it can be considered that D_q is approximately proportional to $1/R^5$. Thus, if R is the smaller, D_q has the larger value, finally results in the red-shift of the emission peak. As the average bond length of Lu1 site (2.706 Å, CN = 9) is somewhat longer than that of Lu2 site (2.543 Å, CN = 7), it is presumed that the larger Ce^{3+} ion relative to Lu^{3+} ion preferably enter the Lu1 site (more space with CN = 9) rather than the Lu2 site (less space with CN = 7). It is well-known that there are several factors that affect the extent of splitting of the d orbitals by ligands. Among several factors, number and geometry of ligands have an important effect on the magnitude of the crystal field splitting (D_q). In comparison between an octahedral complex (Oh, CN = 6) and a tetrahedral complex Td, CN = 4), it can be shown that for a point-charge model:[29]

$$10\,D_q(Td) = 4/9\,[10D_q\,(Oh)] \qquad (2)$$

According to equation (2), it is evident that the larger Ce^{3+} ion relative to Lu^{3+} ion preferably enter the Lu1 site (more space, CN = 9) and the energy splitting of 5d orbitals of Ce^{3+} ions is larger than that in Lu2 site (less space, CN = 7), implying that the emission band is gradually shifted to the red wavelength region with increasing Ce^{3+} concentration in $Lu_{5-x}Ce_x(SiO_4)_3N$ phosphors.

Furthermore, the PL spectrum of $Lu_{4.97}Ce_{0.03}(SiO_4)_3N$ can be divided into two dotted bands centered at about 456 and 495 nm by using Gaussian fitting, as depicted in Figure 2 (c). In general, the emission of Ce^{3+} ions should contain two bands because of the spin-orbit splitting of the ground state ($^2F_{7/2}$ and $^2F_{5/2}$ states) with an energy difference of about 2000

cm^{-1}.[30] However, the energy difference between 453 and 493 nm was calculated to be 1817 cm^{-1}. Thus, these components can be ascribed to the contributions of Ce^{3+} ions at two different luminescence centers, which is in consistent with the structure of Lu$_5$(SiO$_4$)$_3$N. As far as we know, the emission position of Ce^{3+} ions is strongly affected by their local crystal environment, and the following equation can be used to determine the sites of Ce^{3+}:[31]

$$E = Q\left[1 - \left(\frac{V}{4}\right)^{\frac{1}{V}} 10^{-\frac{n \times Ea \times r}{80}}\right]$$

(3)

in which E represents the position of Ce^{3+} ion emission peak (cm^{-1}), Q is the energy position of the lower d-band edge for the free ions (50000 cm^{-1} for Ce^{3+}), V stands for the valence of Ce^{3+} (V = 3 for Ce^{3+}), n is the number of anions in the immediate shell around Ce^{3+} ion, r is the effective radius of the host cations (La^{3+}) replaced by Ce^{3+} ion (Å), and E_a is the electron affinity of the atoms that form anions in eV, which is constant in the same host. The effective ionic radius of Lu^{3+} with nine-coordination is larger than that with seven-coordination. Therefore, the emission peaks at 453 nm and 555 nm are attributed to Ce^{3+} ions with nine-coordination and seven-coordination as shown in the inset of Figure 2 (c).

3.3 Crystal structure of Lu$_5$(SiO$_4$)$_3$N: Ce^{3+}, Tb^{3+} phosphors
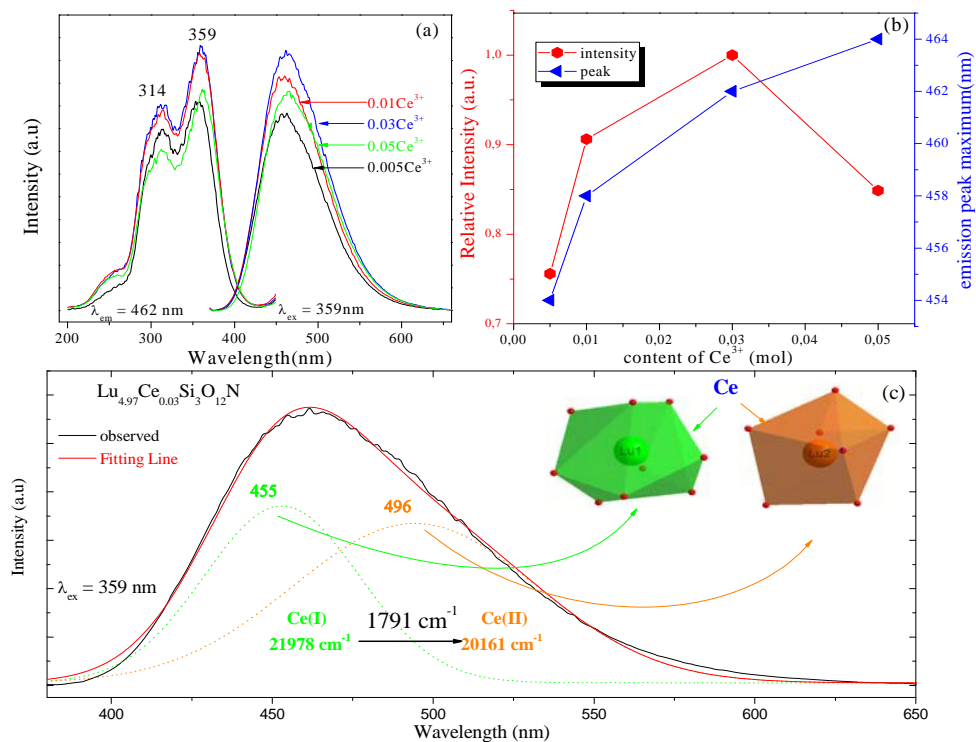
Figure 2. The PLE and PL spectra of Lu$_{5-x}$(SiO$_4$)$_3$N: xCe^{3+} **(a)**; The relative emission intensity and emission peak maximum (nm) as a function of Ce^{3+} concentration **(b)**; PL spectrum of Lu$_{4.97}$Ce$_{0.03}$(SiO$_4$)$_3$N fitted by Gaussian functions under the excitation of 359 nm **(c)**.
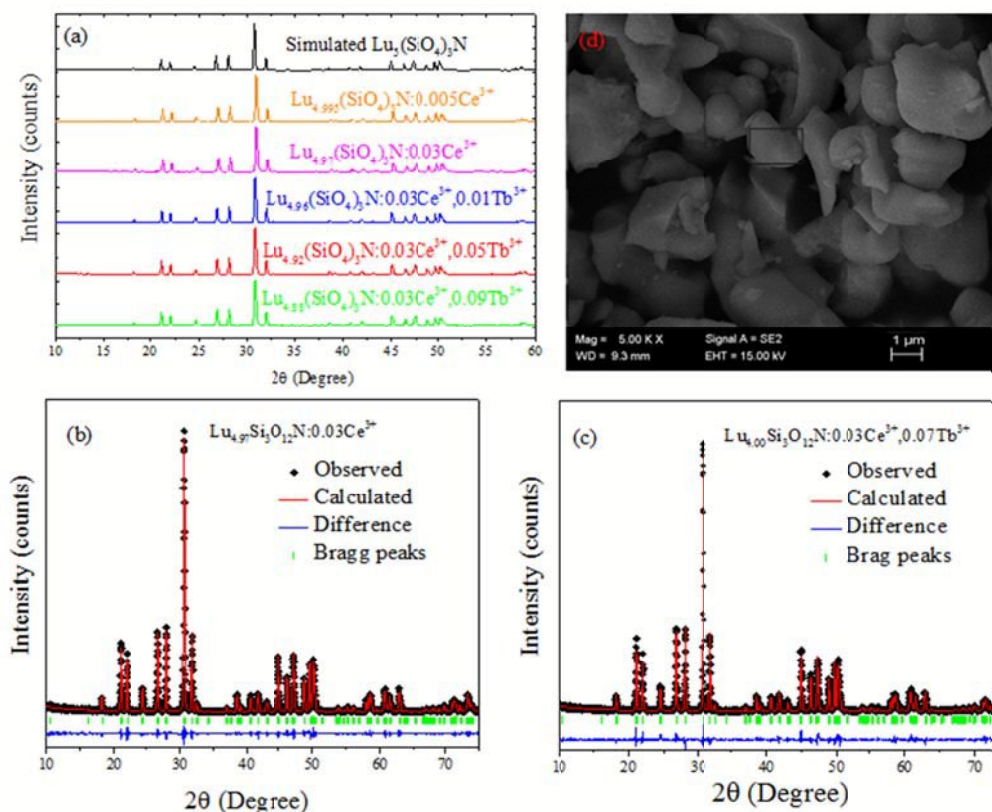
Figure 3. The XRD patterns of $Lu_{4.995}(SiO_4)_3N$: $0.005Ce^{3+}$, $Lu_{4.97}(SiO_4)_3N$: $0.03Ce^{3+}$, $Lu_{4.96}(SiO_4)_3N$: $0.03Ce^{3+}$, $0.01Tb^{3+}$, $Lu_{4.92}(SiO_4)_3N$: $0.03Ce^{3+}$, $0.05Tb^{3+}$, $Lu_{4.88}(SiO_4)_3N$: $0.03Ce^{3+}$, $0.09Tb^{3+}$, as well as the simulated $Lu_5(SiO_4)_3N$ obtained from the structure refinement **(a)**; Powder XRD patterns for Rietveld structure analysis of the selected $Lu_{4.97}Ce_{0.03}(SiO_4)_3N$ **(b)** and $Lu_{4.90}Ce_{0.03}Tb_{0.07}(SiO_4)_3N$ **(c)** phosphors based on the simulated $Lu_5(SiO_4)_3N$ phase model. Solid red lines are calculated intensities, and the black circles are the observed intensities, and blue solid lines for the difference between the observed and the calculated intensities, and short green vertical lines below the profiles stand show the position of Bragg reflections of the calculated pattern; SEM image of $Lu_{4.97}(SiO_4)_3N$: $0.03Ce^{3+}$ **(d)**.

With $4f$–$4f$ forbidden transitions, Tb^{3+} can be effectively sensitized by Ce^{3+}, which can make the emission color of phosphors tunable. Beside, phase purity is an important factor for phosphors to have stable luminescence properties. Thus, some $Lu_{5-x-y}(SiO_4)_3N$: xCe^{3+}, yTb^{3+} phosphors were selected for XRD measurements. Figure 3 (a) shows the XRD patterns of $Lu_{4.995}(SiO_4)_3N$: $0.005Ce^{3+}$, $Lu_{4.97}(SiO_4)_3N$: $0.03Ce^{3+}$, $Lu_{4.96}(SiO_4)_3N$: $0.03Ce^{3+}$, $0.01Tb^{3+}$, $Lu_{4.92}(SiO_4)_3N$: $0.03Ce^{3+}$, $0.05Tb^{3+}$, $Lu_{4.88}(SiO_4)_3N$: $0.03Ce^{3+}$, $0.09Tb^{3+}$, as well as the simulated $Lu_5(SiO_4)_3N$ obtained from the cell refinement. It is shown that all XRD peaks of the samples are consistent with the simulated data for $Lu_5(SiO_4)_3N$, indicating that all the samples are single-phase and the doped Ce^{3+} or Tb^{3+} ions were successfully introduced in the $Lu_5(SiO_4)_3N$ host lattice. In order to better understand the phase structure and purity of the Ce^{3+}/Tb^{3+} doped phosphors, Rietveld refinements were taken for $Lu_{4.97}Ce_{0.03}(SiO_4)_3N$ and $Lu_{4.90}Ce_{0.03}Tb_{0.07}(SiO_4)_3N$ phosphors. The Ce^{3+} or Tb^{3+} ions were supposed to occupy both sites of Lu ions. The refinements were stable and gave low R-factors shown in Figure 3 (a), Figure 3 (b), and Table 5. Besides, the lattice constants of $Lu_{4.97}Ce_{0.03}(SiO_4)_3N$ and $Lu_{4.90}Ce_{0.03}Tb_{0.07}(SiO_4)_3N$ is close to that of $Lu_5(SiO_4)_3N$, indicating that the doped Ce^{3+} or Tb^{3+} ions did not cause any significant changes in the crystal lattice of $Lu_5(SiO_4)_3N$.

The SEM image of $Lu_{4.97}(SiO_4)_3N$: $0.03Ce^{3+}$ was demonstrated in Figure 3 (d), and the phosphor was also analyzed by EDS (Table 4). It is found that the particles have smooth morphology with diameters of the particles between 1 and 6 µm. In addition, the EDS results indicated the presence of Ce^{3+} in the sample.

3.4 Energy transfer investigations in $Lu_{4.97-y}(SiO_4)_3N$: $0.03Ce^{3+}$, yTb^{3+}

Figure 4 presents PLE and PL spectra of $Lu_{4.97}(SiO_4)_3N$: $0.03Ce^{3+}$ (a), $Lu_{4.97}(SiO_4)_3N$: $0.03Tb^{3+}$ (b), and $Lu_{4.94}(SiO_4)_3N$: $0.03Ce^{3+}$, $0.03Tb^{3+}$ (c). The PLE spectrum of $Lu_{4.97}(SiO_4)_3N$: $0.03Tb^{3+}$ presents a broad band from 225 to 314 nm with a maximum at 270 nm corresponding to the $4f^8$–$4f^7$5d transition of Tb^{3+}. As illustrated in the inset of Figure 4 (b), there are some weak lines at 341, 353, and 376 nm, corresponding to the transitions from the $^7F_6$ ground state to the excited states ($^5D_{1,0}$, ^5G_J, $^5L_{10}$ levels) of Tb^{3+} ions. Under 270 nm excitation, $Lu_{4.97}(SiO_4)_3N$: $0.03Tb^{3+}$ can emit strong green light, and the obtained emission spectrum gives typical characteristic transitions of Tb^{3+} ions, which are situated at about 417 nm ($^5D_3$–$^7F_5$), 440 nm ($^5D_3$–$^7F_4$), 491 nm ($^5D_4$–$^7F_6$), 547 nm ($^5D_4$–$^7F_5$), 589 nm ($^5D_4$–$^7F_4$), and 623 nm ($^5D_4$–$^7F_3$).[32, 33] As shown in Figure 4 (c), it includes three peaks located at 270, 314, and 359 nm in the

ARTICLE

excitation spectrum of $Lu_{4.94}(SiO_4)_3N$: $0.03Ce^{3+}$, $0.03Tb^{3+}$ phosphor monitored with 462 nm. According to the above discussions, the peak at 265 nm belongs to the $4f^8–4f^75d^1$ transition of Tb^{3+}, while the peaks at 306 and 365 nm correspond to the $4f–5d$ transition of Ce^{3+}. Upon the excitation of 359 nm, both the emission of Ce^{3+} and Tb^{3+} can be observed in the PL spectrum of the co-doped $Lu_{4.94}(SiO_4)_3N$: $0.03Ce^{3+}$, $0.03Tb^{3+}$ sample as depicted in Figure 4 (c). Based on the Dexter theory, energy transfer requires a spectral overlap between the donor emission band and the acceptor excitation band.[34] The inset of Figure 4 (c) shows the PLE spectrum of $Lu_{4.97}(SiO_4)_3N$: $0.03Tb^{3+}$ and PL spectrum of $Lu_{4.97}(SiO_4)_3N$: $0.03Ce^{3+}$ ranging from 380 to 400 nm. It is clear that there is a spectral overlap in the range from 386 to 396 nm in combination with the emission band of Ce^{3+} (donor) and the excitation of Tb^{3+} (acceptor). Therefore, the energy transfer from Ce^{3+} to Tb^{3+} may occur in $Lu_5(SiO_4)_3N$ host.

As discussed above, the optimum doping concentration of Ce^{3+} is 0.03 (mol). In order to further investigate the energy transfer process between the Ce^{3+} and Tb^{3+} ions in $Lu_5(SiO_4)_3N$ host, a series of $Lu_{4.97-y}(SiO_4)_3N$:$0.03Ce^{3+}$, yTb^{3+} (y = 0, 0.01, 0.03, 0.05, 0.07, and 0.09) phosphors were prepared. Figure 4 (d) presents the emission spectra of $Lu_{4.97-y}(SiO_4)_3N$: $0.03Ce^{3+}$, yTb^{3+} phosphors with an excitation of 359 nm. It is clear that both the emission peaks of Ce^{3+} and Tb^{3+} can be observed in the as-prepared $Lu_{4.97-y}(SiO_4)_3N$: $0.03Ce^{3+}$, yTb^{3+} phosphors except for $Lu_{4.97}(SiO_4)_3N$: $0.03Ce^{3+}$. As illustrated in Figure 4 (e), the relative emission intensities of the Ce^{3+} ions decreased remarkably, whereas the relative emission intensities of Tb^{3+} increased first with the Tb^{3+} concentration. Then, the emission intensity of Tb^{3+} in $Lu_{4.97}(SiO_4)_3N$: $0.03Ce^{3+}$,$0.09Tb^{3+}$ decreased slightly with further increasing concentration of Tb^{3+}, ascribed to the concentration quenching effect.

Table 5. Refinement parameters for $Lu_{4.97}Ce_{0.03}(SiO_4)_3N$ and $Lu_{4.90}Ce_{0.03}Tb_{0.07}(SiO_4)_3N$ from the Rietveld refinement using X-ray powder diffraction data at room temperature.

Samples	$Lu_{4.97}Ce_{0.03}Si_3O_{12}N$	$Lu_{4.90}Ce_{0.03}Tb_{0.07}Si_3O_{12}N$
Space group	$P6_3/m$(176)	$P6_3/m$(176)
a, Å	9.6989(33)	9.69885(25)
c, Å	7.2489(27)	7.2592(03)
V, Å^3	590.35(5)	591.99(24)
2θ-interval, °	10-75	10-75
Rwp, %	9.56	9.40
Rp, %	6.73	7.09
$\chi2$	1.85	2.43

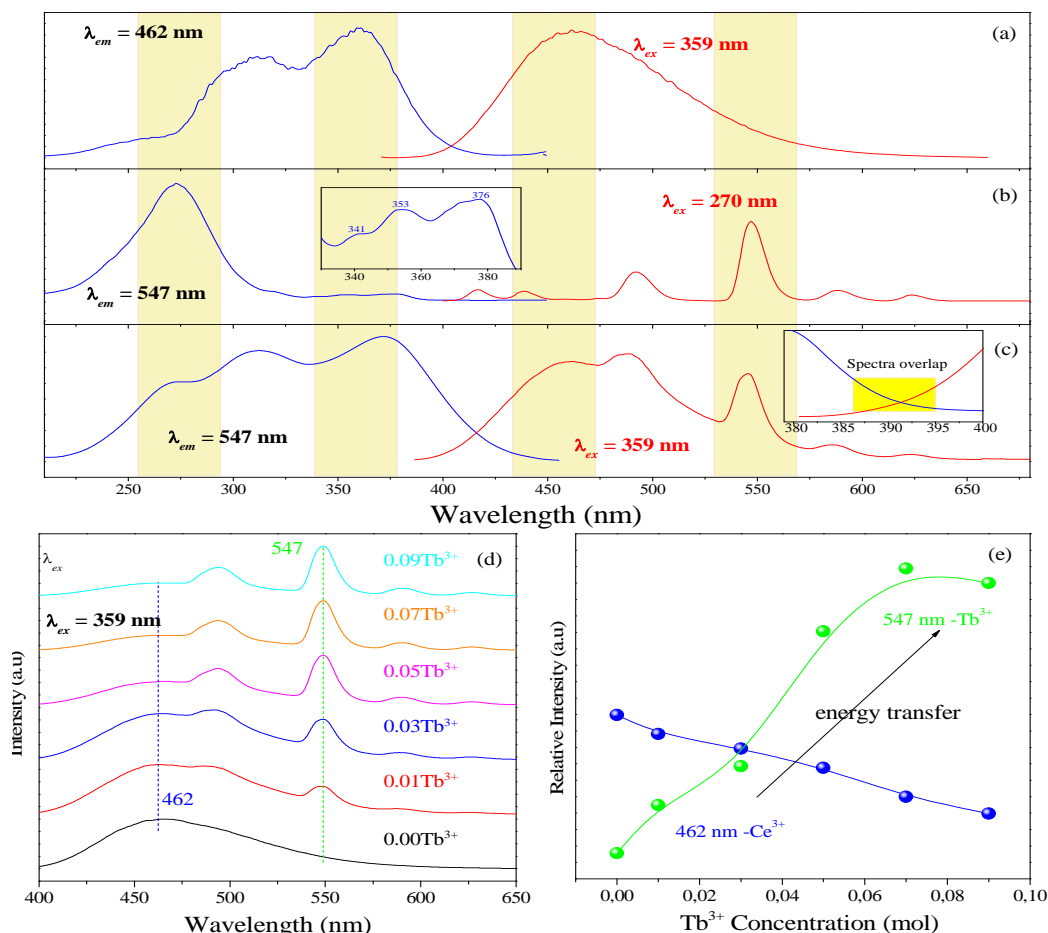**Figure 4.** The PL excitation and emission spectra of $Lu_{4.97}(SiO_4)_3N$: $0.03Ce^{3+}$ **(a)**; the PL excitation and emission spectra of $Lu_{4.97}(SiO_4)_3N$: $0.03Tb^{3+}$**(b)**, and the inset of **(b)** shows PLE spectra of $Lu_{4.97}(SiO_4)_3N$: $0.03Tb^{3+}$ ranging from 330 nm to 390 nm; the PL excitation and emission spectra of $Lu_{4.94}(SiO_4)_3N$: $0.03Ce^{3+}$, $0.03Tb^{3+}$ **(c)**, and the inset of **(c)** illustrates the PLE spectrum of $Lu_{4.97}(SiO_4)_3N$: $0.03Tb^{3+}$ and PL spectrum of $Lu_{4.97}(SiO_4)_3N$: $0.03Ce^{3+}$ in the range from 380 to 400 nm; the emission spectra of $Lu_{4.97-y}(SiO_4)_3N$: $0.03Ce^{3+}$, yTb^{3+} (y = 0, 0.01, 0.03, 0.05, 0.07, and 0.09) phosphors with an excitation wavelength of 359 nm **(d)**; Relative emission intensities of Ce^{3+} and Tb^{3+} ions in $Lu_{4.97-y}(SiO_4)_3N$: $0.03Ce^{3+}$, yTb^{3+} **(e)**.

To further confirm the energy transfer between Ce^{3+} and Tb^{3+}, the decay curves of $Lu_{4.97-y}(SiO_4)_3N$:$0.03Ce^{3+}$, yTb^{3+} (y = 0, 0.01, 0.03, and 0.05) were collected (λ_{ex} = 370 nm, λ_{em} = 462 nm), which is shown in Figure 5(d). Generally, energy transfer from $Ce^{3+}$to Tb^{3+} belongs to multipolar interaction between donor and acceptor ions. According to Dexter theory, the energy transfer probability through multipolar interaction can be calculated by equation (4): [35]

$$P(R) \propto \frac{Q_A}{R^b \tau_D} \int \frac{f_D(E)F_A(A)}{E^c} \, dE \qquad (4)$$

in which b and c are constant, P represents the energy transfer probability, τ_D is the decay time of the donor (activator Ce^{3+}) emission, Q_A stands for the total absorption cross-section of the acceptor, and R is the distance between the donor (Ce^{3+}) and the acceptor (Tb^{3+}). Thus, the energy-transfer probability P is inversely proportional to the decay time τ_D. Additionally, the

decay curves for all the phosphors can be well fitted with a second-order exponential decay mode using equation (5): [36]

$$I(t) = A_1 \, exp(-t/\tau_1) + A_2 \, exp(-t/\tau_2) \qquad (5)$$

where $I(t)$ is the luminescence intensities at times t, A_1 and A_2 are fitting constants, and τ_1 and τ_2 stand for the decay times for the exponential components. Based on equation (6), the average life times (τ^*) can be calculated using the parameters in equation (5). [37]

$$\tau^* = (A_1 \tau_1^2 + A_2 \tau_2^2) / (A_1 \tau_1 + A_2 \tau_2) \qquad (6)$$

As illustrated in the inset of Figure 5 (d), all the R^2 values are higher than 98%, which indicated that the fitting is relatively good. Therefore, τ^* for $Lu_{4.97-y}(SiO_4)_3N$:$0.03Ce^{3+}$, yTb^{3+} (y = 0, 0.01, 0.03, and 0.05) were determined to be 4.41, 3.74, 2.10, and 1.67 ns, respectively. Obviously, the decay time decreases gradually with the increase of Tb^{3+} concentration, which
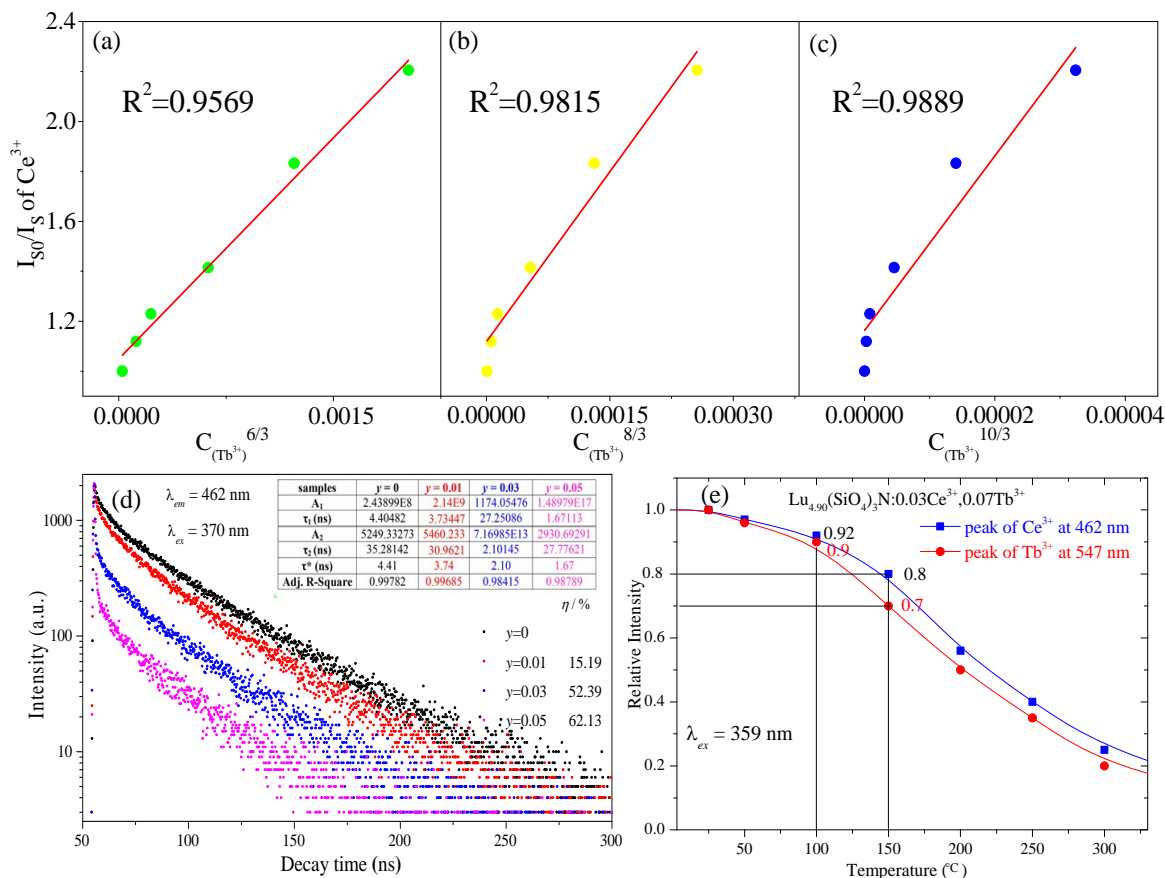
Figure 5. Dependence of I_{S0}/I_S of Ce^{3+} on $C^{6/3}$ **(a)**; $C^{8/3}$ **(b)**; $C^{10/3}$ **(c)**; Decay curves of Ce^{3+} emission in $Lu_{4.97-y}(SiO_4)_3N:0.03Ce^{3+}$, yTb^{3+} ($y = 0$, 0.01, 0.03, and 0.05) phosphors under excitation at 370 nm monitored at 462 nm at room temperature, and the inset depicts the fitted lifetimes, fitting parameters, as well as the energy transfer efficiency calculated on the basis of lifetimes **(d)**; The relative emission intensities centered at 462 nm (Ce^{3+}) and 547 nm (Tb^{3+}) of the selected sample as a function of temperature ranging from 25 ^{o}C to 300°C **(d)**.

strongly demonstrates the energy transfer from the from Ce^{3+} to Tb^{3+}.

In general, the energy transfer efficiency η_T from a sensitizer to an activator can also be expressed using the following equation by Paulose et al.:[38, 39]

$$\eta_T = 1 - \tau_S/\tau_0 \qquad (7)$$

where τ_S and τ_0 represent the luminescence lifetimes of the sensitizer Ce^{3+} ion in the presence and the absence of the activator Tb^{3+} ion, respectively. On the basis of the above calculated average values of the lifetimes (τ^*), the energy transfer efficiency η_T can be calculated to be 15.19%, 52.39%, and 62.13% as given in Figure 5 (d). With the increase of Tb^{3+} concentration, the value of η_T increased gradually and reached the maximum of 62.13% when y equals to 0.05. Thus, an efficient energy transfer from Ce^{3+} to Tb^{3+} must have occurred in $Lu_{4.97-y}(SiO_4)_3N:0.03Ce^{3+}$, yTb^{3+}.

As we know, there are two main aspects that are responsible for the resonance energy transfer mechanism: one

is the multipolar interaction and the other is the exchange interaction. Meanwhile, the critical distance between the sensitizer and the activator should be shorter than 5 Å for the exchange interaction. To further determine the energy transfer mechanism in $Lu_5(SiO_4)_3N$, the critical distance (R_C) between Ce^{3+} and Tb^{3+} ions was calculated using the concentration quenching method proposed by Blasse.[40, 41]

$$R_c \approx 2\left(\frac{3V}{4\pi x_c N}\right)^{\frac{1}{3}} \qquad (8)$$

where x_c is critical concentration, V corresponds to the volume of the unit cell, and N stands for the number of host cations in the unit cell. For the $Lu_5(SiO_4)_3N$ host, $N=10$, and V is estimated to be 589.87 $Å^3$ as shown in Table 1. Besides, the critical concentration is about 0.10 (mol) from the overall concentration of the Ce^{3+} (0.03) and Tb^{3+} (0.07). Therefore, the critical distances R_C of energy transfer can be estimated to be about 10.405 Å ($x_c = 0.10$) on the basis of the above equation. The value of R_C is much larger than 5 Å, which indicated the

electric multipolar interaction can take place for the energy transfer between Ce^{3+} and Tb^{3+} in $Lu_5(SiO_4)_3N$ host lattice. In addition, the multipolar interaction can be determined by Dexter's energy-transfer expressions and Reisfeld's approximation given as follows.:[42, 43]

$$\eta_0 / \eta \propto C^{n/3} \tag{9}$$

where η_0 and η stand for the luminescence quantum efficiency of Ce^{3+} in the absence and presence of Tb^{3+}, C corresponds to the total content of Ce^{3+} and Tb^{3+}, $n = 6$, 8, and 10, respectively. The value η_0/η is approximately calculated by the ratio of related luminescence intensities as (I_0/I_S). Besides, $n = 6$, 8, and 10 correspond to the electric multipolar interaction of the electric dipole–dipole, dipole-quadrupole, and quadrupole–quadrupole, respectively. The $I_0/I_S - C^{n/3}$ plots are further illustrated in Figure 5 (a), (b), and (c). By comparing the values of the fitting factors R^2, the optimal linear relationship is obtained when $n = 10$ ($R^2 = 0.9894$). This indicates that the quadrupole–quadrupole interaction should be mainly responsible for the energy transfer from Ce^{3+} to Tb^{3+} ions in $Lu_{4.97-y}(SiO_4)_3N:0.03Ce^{3+}$, yTb^{3+}.

As we know, the thermal stability of phosphor is one of the most important technological parameters for its application. Therefore, the $Lu_{4.90}(SiO_4)_3N:0.03Ce^{3+}$, $0.07Tb^{3+}$ was selected for PL measurement under 359 nm excitation at different temperatures ranging from 25 ℃ to 300 ℃. The relative emission intensities centered at 462 nm (Ce^{3+}) and 547 nm (Tb^{3+}) of the selected sample as a function of temperature are shown in Figure 5(e). The relative PL intensities centered at 462 nm (Ce^{3+}) and 547 nm (Tb^{3+}) decrease to 80% and 70% of the initial values (25 ^{o}C) with the temperature rising to 150 ^{o}C, implying that the sample has high thermal stability.

3.5 CIE chromaticity diagram and quantum efficiency (QE) of $Lu_{4.97-y}(SiO_4)_3N: 0.03Ce^{3+}$, yTb^{3+}

Table 6. CIE Coordinates for $Lu_{4.97-y}(SiO_4)_3N:0.03Ce^{3+}$, yTb^{3+} (y = 0, 0.01, 0.03, 0.05, 0.07, and 0.09) (λ_{ex} = 359 nm).

Samples	CIE (x,y)
y = 0	(0.1480,0.1842)
y = 0.01	(0.1586,0.1937)
y = 0.03	(0.1696,0.2239)
y = 0.05	(0.1783,0.2483)
y = 0.07	(0.2188,0.3549)
y = 0.09	(0.2249,0.3713)
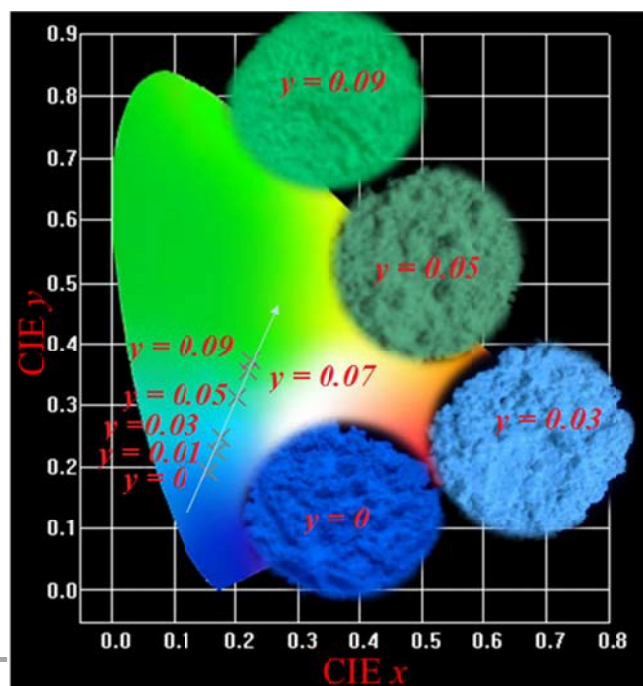
Figure 6. The CIE chromaticity diagram of $Lu_{4.97-y}(SiO_4)_3N:0.03Ce^{3+}$, yTb^{3+} (y = 0, 0.01, 0.03, 0.05, 0.07, and 0.09) phosphors under 359 nm excitation, and the insets of shows the digital photos of the selected samples (y = 0, 0.03, 0.05, and 0.09) under 365 nm UV lamp excitation.

Figure 6 depicts the CIE chromaticity diagram of $Lu_{4.97-y}(SiO_4)_3N:0.03Ce^{3+}$, yTb^{3+} (y = 0, 0.01, 0.03, 0.05, 0.07, and 0.09) phosphors with different Tb^{3+} concentration under 359 nm excitation calculated by PL spectrum, and the insets of Figure 6 shows the digital photos of the selected samples (y = 0, 0.03, 0.05, and 0.09) under 365 nm UV lamp excitation. The CIE coordinates of the $Lu_{4.97-y}(SiO_4)_3N: 0.03Ce^{3+}$, yTb^{3+} phosphors shifted from the blue (0.1480,0.1842) to green (0.2249, 3713) region with Tb^{3+} concentration, as indicated in Table 6. Therefore, the emission color of the phosphors can be tuned by adjusting the doping content of Tb^{3+} ions. In addition, the quantum efficiency of phosphors is another important factor for their application in LED. Therefore, the absolute quantum efficiency (QE) of $Lu_{4.97}(SiO_4)_3N: 0.03Ce^{3+}$ sample was investigated. Under the excitation of 359 nm, the absolute QE for the phosphor was determined to be 42.13%.

4. Conclusions

In summary, novel single-phase $Lu_5(SiO_4)_3N$ compound and $Lu_5(SiO_4)_3N:Ce^{3+},Tb^{3+}$ phosphors with apatite structure were obtained for the first time via a high temperature solid state method with 0.5 MPa atmosphere pressure. The results indicated that $Lu_5(SiO_4)_3N$ crystallized in hexagonal space group $P6_3/m$ with cell parameters $a = b = 9.7005$ Å and $c = 7.2383$ Å. Two non-equivalent lutetium sites exist in $Lu_5(SiO_4)_3N$, that is, Lu(1) with nine coordination and Lu(2) with

ARTICLE Journal Name

seven coordination. The ratio of the number of Lu atoms in Lu(1) and Lu(2) sites is 3:2. The band gap for $Lu_5(SiO_4)_3N$ was 4.12 eV. In the Ce^{3+} doped $Lu_5(SiO_4)_3N: 0.03Ce^{3+}$ compound, the emission peak centered at 462 nm was observed with the Commission International de I'Eclairage (CIE) coordinates of (0.148, 0.184), indicating blue-emission. Remarkably, in Ce^{3+} and Tb^{3+} co-doped $Lu_{4.97-y}(SiO_4)_3N: 0.03Ce^{3+}, yTb^{3+}$ compounds, the color-tunability was observed with increasing Tb^{3+} co-doping rate on moving from blue at Tb^{3+} = 0.00 to green at Tb = 0.09, due to the energy transfer from Ce^{3+} to Tb^{3+} ions being matched well with the decay curve results. The energy transfer process from the Ce^{3+} to Tb^{3+} ions occurs in the host lattice with quadrupole–quadrupole interaction mechanism. The excitation spectra of the $Lu_5(SiO_4)_3N:Ce^{3+},Tb^{3+}$ phosphors give a broad excitation band in the wavelength range from 235 nm to 435 nm. The absolute quantum efficiency (QE) for $Lu_5(SiO_4)_3N: 0.03Ce^{3+}$ was determined to be 42.13%. All the above results demonstrate that $Lu_5(SiO_4)_3N$ could be a platform for modeling a new phosphor and application in the solid-state lighting field and that $Lu_5(SiO_4)_3N: Ce^{3+},Tb^{3+}$ samples could be used as blue-green phosphors.

Acknowledgements

Notes and references

1 Y. Li, W.J. Liu, X.C. Wang, G. Zhu, C. Wang, and Y.H Wang, *Dalton. Trans.*, 2015, **44**, 13196-13203.
2 D. Kim, D. Park, N. Oh, J. Kim, E.D. Jeong, S.J. Jim, S. Kim, and J. C. Park, *Inorg. Chem.*, 2015, **54**, 1325-1336.
3 F. Lu, X. Song, and Q. Liu, 2011, **509**,2099-2104.
4 L. K. Bharat, J.Y. Park, and J.S. Yu., *Chem. Eng. J.*, 2014, **240**, 179-186.
5 M.F. Zhang, Y.J. Liang, S.Y. Xu, Y.L. Zhu, X.Y. Wu, and S.Q. Liu, *CrystEngComm.*, 2016, **18**, 68-76.
6 Z.L. Dong, T.J. White, K. Sun, L.M. Wang, and R.C. Ewing, *J. Am. Chem. Soc.*, 2015, **88**, 184-190.
7 E.N. Bulanov, J.X. Wang, A. V. Knyazev, T. White, M.E. Manyakina, T. Baikie, A.N. Lapshin, and Z.L. Dong, *Inorg. Chem.*, 2015, **54**, 11356-11361.
8 K. Fukuda, T. Asaka, S. Hara, M. Oyabu, A. Berghout, E. Bechade, O. Masson, I. Julien, and P. Thomas, *Chem. Mater.*, 2013, **25**, 2154-2162.
9 Q. F. Guo, L.B. Liao, L.F. Mei, and H.K. Liu, *J. Solid. State. Chem.*, 2015, **226**, 107-113.
10 M. M. Jiao, Y.C. Jia, W. Lu, W.Z. Lv, Q. Zhao, B.Q. Shao, and H.P. You, *J. Mater. Chem. C*, 2014, **2**, 90-97.
11 K. Li, D.L. Geng, M.M. Shang, Y. Zhang, H.Z. Lian, and J. Lin, *J. Phys. Chem. C*, 2014, **118**, 11026-11034.
12 D.L. Geng, H.Z. Lian, M.M. Shang, Y. Zhang, and J. Lin, *Inorg. Chem.*, 2014, **53**, 2230-2239.
13 Y.C. Chiu, T.J. Lee, W.R. Liu, Y.T. Yeh, S.M. Jang, and R.S. Liu, *Opt. Express.*, 2011, **19**, 331-339.
14 G. Z. Chen, L.J. Yin, J.T. Dong, Y.Y. Feng, Y. Gao, W.D. He, Y. Jia, and H.T. Hintzen, *J. Am. Chem. Soc.*, 2016, **99**, 183-190.
15 C.H. Huang, Y.C. Chiu, and W.R. Liu, *Eur. J. Inorg. Chem.*, 2014, **3**, 3674-3680.
16 J.W.H. van Krevel, H.T. Hintzen, R. Metselaar, and A. Meijerink. *J. Alloys. Compd.*, 1998, **268**, 272- 277.
17 X.M. Wang, C.H. Wang, X.J. Kuang, R.Q. Zou, Y.X. Wang, and X.P. Jing, *Inorg. Chem.*, 2012, **51**, 3540-3547.
18 F.C. Lu, L.J. Bai, Z.P. Yang, and X.N. Han, *Mater. Lett.*, 2015, **151**, 9-11.
19 X. Xu, C. Cai, L.Y. Hao, Y.C. Wang, and Q.X. Li, *Mater. Chem. Phys.*, 2009, **118**, 270-272.
20 J. takahashi, H. Yamane, M. Shimad, Y. Yamamoto, N. Hirosaki, M. Mitomo, K. Oikawa, S. Torii, and T. Kamiyama, *J. Am. Chem. Soc.*, 2002, **85**, 2072-2077.
21 A.C. Larson, and R.B. Von Dreele, *Los Alamos National Laboratory*, Report LAUR: Los Alamos, 1986,86-748.
22 G. Kresse, and G. Furthmuller, *Comput. Mater. Sci.*, 1996, **6**, 15-50.
23 F.C. Lu, and L.J. Bai, *J. Am. Ceram. Soc.*, 97, 2397-2400.
24 B. Dierre, R.J. Xie, N. Hirosaki, and T. Sekiguchi, *J. Mater. Res.*, 2007, **22**, 1933-1941.
25 S. Titeux, M. Gervais, P. Verdier, and Y. Laurent, *Mater. Sci. Forum.*, 2000, **325-326**, 17-20.
26 M. Yang, H.P. You, K. Liu, Y.H. Zheng, N. Guo, and H.J. Zhang, *Inorg. Chem.*, 2010, **49**, 4996-5002.
27 X.H. Gong, J.H. Huang, Y.J. Chen, Y.F. Lin, Z.D. Luo, and Y.D. Huang, *Inorg. Chem.*, 2014, **53**, 6607-6614.
28 C.L. Zhao, Z.G. Xia, and S.X. Yu, *J. Mater. Chem. C*, 2014, **2**, 6032-6039.
29 J.E. Huheey, E.A. Keiter, and R.L. Keiter, R. L. Inorganic Chemistry: Principles of Structure and Reactivity; Harper Collins College Publishers: New York, 1993.
30 H.B. Liang, H.H. Lin, G.B. Zhang, P. Dorenbos, and Q. Su, *J. Lumin.*, 2011, **131**, 194-198.
31 L.G. Van Uitert, *J. Lumin.*, 1984, **29**, 1-9.
32 T. Grzyb, K. Kubasiewicz, A. Szczeszak, and S. Lis, *Dalton Trans.*, 2015, **44**, 4063-4069.
33 L. Liu, Y.M. Liang, L.L. Li, L.C. Zou, and S.C. Gan, *CrystEngComm.*, 2015, **17**, 7754-7761.
34 Y. Chen, Y. Li, J. Wang, M.M. Wu, and C.X. Wang, *J. Phys. Chem. C*, 2014, **118**, 12494-12499.
35 D. L. Dexter, *J. Chem. Phys.*, 1953, **21**, 836-850.
36 D Geng, M. Shang, Y. Zhang, H. Lian, and J. Lin, *Dalton Trans.*, 2013, **42**, 15372-15380.
37 C. H. Huang, T. M. Chen, W. R. Liu, Y. C. Chiu, Y. T. Yeh, and S. M. Jang, *ACS Appl. Mater. Interfaces*, 2010, **2**, 259-264.
38 P. I. Paulose, G. Jose, V. Thomas, N. V. Unnikrishnan, and M. K. R. Warrier, *J. Phys. Chem. Solids*, 2003, **64**, 841-846.
39 W.Z. Lv, M.M. Jiao, Q. Zhao, B.Q. Shao, W. Lu, and H.P. You, *Inorg. Chem.*, 2014, **53**, 11007-11014.
40 G. Blasse, *J. Solid. State. Chem.*, 1986, **62**, 207-211.
41 G. Blasse, *Phy. Let. A*, 1968, **28**, 444-445.
42 L.H. Liu, L. Wang, C.N. Zhang, Y.J. Cho, B. Dierre, N. Hirosaki, T. Sekiguchi, and R.J. Xie, *Inorg. Chem.*, 2015, **54**, 5556-5565.
43 C.H. Huang, T.W. Kuo, and T.M. Chen, *ACS Appl. Mater. Interfaces*, 2010, **2**, 1395-1399.